Effects of an oxygen environment on the electrical properties of a single CdS nanobelt device

2011 Nanotechnology 22 135702

(http://iopscience.iop.org/0957-4484/22/13/135702)

Nanotechnology **22** (2011) 135702 (7pp) doi:10.1088/0957-4484/22/13/135702

Effects of an oxygen environment on the electrical properties of a single CdS nanobelt device

Jin An[1], Kun Xue[1,2], Weiguang Xie[1], Quan Li[3] and Jianbin Xu[1,4]

[1] Department of Electronic Engineering and Material Science and Technology Research Center, The Chinese University of Hong Kong, Shatin, NT, Hong Kong SAR
[2] School of Physics and Australian Research Council Centre of Excellence for Quantum Computation and Communication Technology, University of New South Wales, Sydney, NSW 2052, Australia
[3] Department of Physics, The Chinese University of Hong Kong, Shatin, NT, Hong Kong SAR

E-mail: kxue@ee.cuhk.edu.hk and jbxu@ee.cuhk.edu.hk

Received 11 October 2010
Published 22 February 2011
Online at stacks.iop.org/Nano/22/135702

Abstract
The influence of the oxygen environment on the transport behavior of a cadmium sulfide (CdS) single crystal nanobelt is investigated by device performance under various light illuminations and oxygen partial pressures. The CdS nanobelt shows superior photo response in the visible light region and the conductance is sensitive to the oxygen environment. The results show that when exposed to oxygen, the surface chemisorbed oxygen species and their interactions with surface defects will significantly affect the conductivity by decreasing the carrier concentrations and reducing the mobility. The effect is explained by surface band bending which is observed by surface potential measurement. Furthermore, we show that the height of the nanobelt is one of the critical factors that greatly affects the conductance due to the intrinsic belt-like geometry.

(Some figures in this article are in colour only in the electronic version)

1. Introduction

1D or quasi-1D semiconductor nanostructures, such as nanotubes (NTs), nanowires (NWs) or nanobelts (NBs), have been extensively studied due to their excellent electronic and optical properties. Among these, II–VI compound semiconductors cadmium sulfide(CdS) (with a direct band gap of 2.42 eV) NWs/NBs have already shown promising properties for building nanometer-scale devices, such as field effect transistors (FETs) [1–3], semiconductor lasers [4], metal–semiconductor–metal (MSM) photodiodes [5] and avalanche photodiodes (APDs) [6]. It is reported that the contacts [7–10], surface-to-volume ratio [11], and heterostructures [12] all have effects on the carrier transport behaviors. Specifically, surface related phenomena (such as surface adsorbates, surface states/defects) play a crucial role in carrier transport for nanostructured devices because of the large surface-to-volume ratio of NWs/NBs compared with their bulk counterparts. Since their environments would substantially modify the surface [11], a detailed understanding of the dependence of carrier transport on the ambient will facilitate control of surface defects/states, which is essential for optimizing the performance of NW/NB devices and designing future novel nanometer-scale chemical or biochemical sensors.

In this work we investigate the changes in the electron transport properties of the CdS NB photoconductors and FETs in relation to the oxygen environment as well as NB geometry. It shows that photoconductivity of a CdS NB is sensitive to the oxygen concentration and the height of the NB. The transfer curves of the device support that the oxygen species induce a decrease in the carrier concentration inside the NBs, which is related to the chemically adsorbed negative oxygen ions on the CdS surface. Finally, scanning surface potential microscopy (SSPM) is used to confirm the surface band bending status.

2. Experimental details

CdS NBs were synthesized on a silicon substrate by the vapor liquid solid (VLS) chemical vapor deposition (CVD)

[4] Author to whom any correspondence should be addressed.

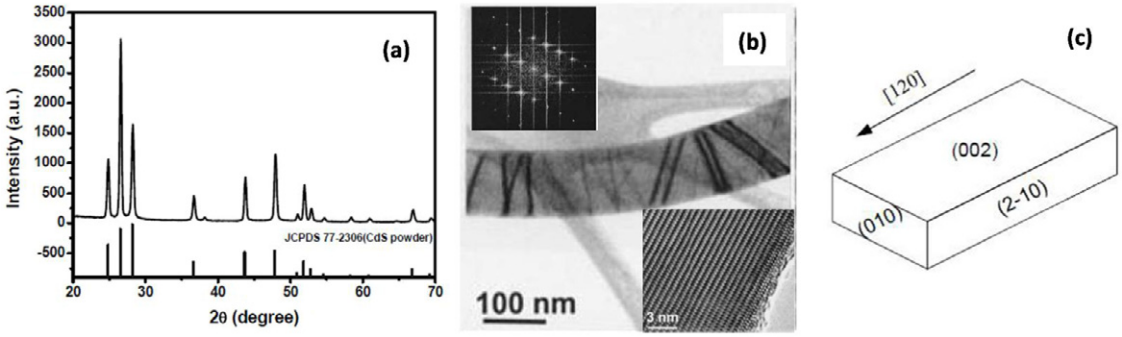

Figure 1. (a) XRD pattern of the CdS NBs. (b) TEM image of a CdS NB on a carbon grid. The inset at the lower right shows the high-resolution image of the CdS NB and the upper left shows the corresponding diffraction pattern. The electron beam is aligned along the CdS {100} axis. (c) A schematic of the growth structure of the CdS NB.

technique without a Au catalyst [13, 14]. The geometry of the NBs was determined by atomic force microscopy (AFM) and scanning electron microscopy (SEM). X-ray diffraction (XRD) and transmission electron microscopy (TEM) were employed to obtain the structural information. The CdS NBs were then dispersed in 2-propanol (IPA) solvent and deposited on a SiO_2 dielectric layer. The SiO_2 (300 nm) was thermally grown on low resistivity (0.001–0.005 Ω cm) p-type silicon substrate, which was used as the bottom gate and aluminum was evaporated on the backside as the gate electrode. The source and drain electrodes of the CdS NB FET were patterned on both ends of a selected CdS NB by photolithography. Electrodes (Ti 20 nm/Au 100 nm) were subsequently deposited to form the electrical contacts. The typical channel length (L) was about 4 μm; the channel width was determined by the width of the CdS NB (hundreds of nanometers). The electrical measurements were performed with the device inside a cryostat. The gas pressure and concentration inside the cryostat were adjusted by pumping and filling the cryostat with dry oxygen or dry nitrogen with a purity of ∼99.995%. Illumination was achieved with an argon laser (wavelength ∼488 nm) through the quartz window of the cryostat and the power intensity of the laser remained constant during the measurement. Further, the surface potential study of the CdS was performed earlier on the Veeco Dimension 3100 AFM operated in the scanning surface potential microscopy (SSPM) mode.

3. Results and discussion

3.1. Crystallographic structure of the CdS NBs

Unlike NWs or NTs, NBs have a rectangular cross-section with well-defined geometry and high crystallinity. The AFM investigation confirmed that the CdS NBs have belt-like geometry with a typical length of tens of micrometers, a width of hundreds of nanometers and a thickness of tens of nanometers. Figure 1(a) shows the XRD results for the NBs which agree well with those for CdS crystal. Figure 1(b) presents a TEM image of a NB, and transmission electron diffraction (TED) patterns confirm that the NBs are single crystalline. A universal growth direction (along the hexagonal [120] direction) is evidenced by the Fourier transform (upper inset) from the high-resolution image (lower inset). The termination facets are (002), (010) and (210) planes as illustrated in figure 1(c). From the HRTEM images, it is found that there is a very thin amorphous layer (less than 1 nm) covering the CdS NB surface, very probably an oxide layer.

3.2. Photocurrent response

A single crystal CdS NB FET with a floating back gate will act as a two-terminal photodetector. Figure 2(a) shows the photocurrent response (I–V characteristics) for this configuration. The dark current of the CdS device is quite small. However, when illuminated with a blue laser (λ = 488 nm), the conductivity increases by more than 10^4 times. The large change of conductivity under the above-band gap illumination may originate from the concentration change of the photo-generated carriers inside the NB or the change in effective barrier height of the metal–semiconductor contacts [5, 15–17]. By using photo-assisted SSPM, we verified that both processes make important contributions to the photoconductivity: in the dark or under weak illumination, a large bias potential is consumed by the metal–semiconductor junction; under high illuminations, the CdS device channel dominates the whole device conductance [18].

The cathodoluminescence (CL) spectrum for the same device is shown in figure 2(b). The CL emission peak is at ∼2.4 eV, corresponding to the near-band-edge emission of CdS (2.42 eV). No quantum confinement effect is observed since the NB geometry is far beyond its exciton Bohr radius (∼2.9 nm) [19]. A small CL peak is observed at ∼700 nm, which may result from the transitions from defects inside the NB bulk. No such peak is observed in the photocurrent spectrum. The reason for this is that the CL emission excited by the ∼20 kV electron beam mainly originates from the NB bulk due to the penetration depth of the electrons [20]. However, the photocurrent is more sensitive to the NB surface status.

3.3. Photocurrent decay versus ambient

Normalized temporal photocurrents with different ambient environments are shown in figure 3(a). The illumination

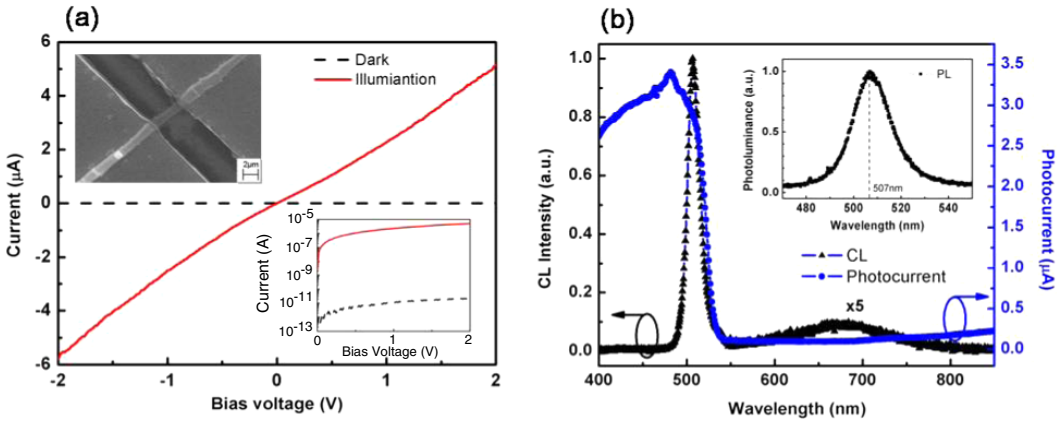

Figure 2. (a) Typical current–voltage curve for the single CdS NB device, the lower-right inset shows the logarithm of current; the upper-left inset is the scanning electron microscopy image for the given device; the channel length is about 4 μm. (b) The photocurrent response and cathodoluminescence spectrum for one given CdS device.

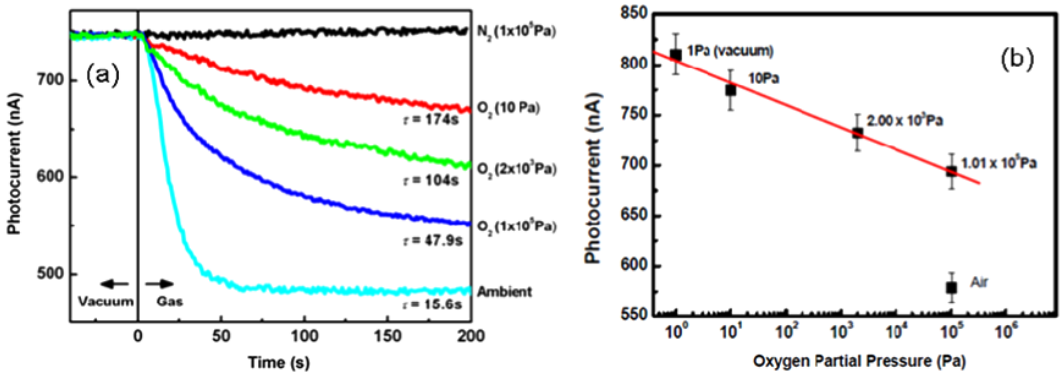

Figure 3. (a) Normalized temporal photocurrents as a function of time under different oxygen partial pressures with a bias voltage of 4 V. (b) The steady photocurrent under different oxygen partial pressures.

intensity remains constant. Before introducing gas, the device was stored in a vacuum (∼1 Pa) for long enough to reach a steady photocurrent. The temporal photocurrent responses are significantly affected by the gas species and concentrations. Once exposed to the O_2, the photocurrent starts to drop; however, when exposed to inert N_2 or Ar gas, no detectable changes were observed. The higher the oxygen concentration is, the faster the photocurrent drops and the smaller the final steady photocurrent. The photocurrent change can be fitted by an exponential decay: $I_{on}/I_{max} = (1 - A)\exp(-t/\tau_d) + A$, where A is the normalized steady-state photocurrent and τ_d is the decay time constant. With the oxygen partial pressure from 10 to 10^5 Pa, τ_d drops from 174 to 47 s. The change in steady-state photocurrent with oxygen partial pressure is illustrated in figure 3(b). The photocurrent increases monotonically with the decrease of oxygen partial pressure. Since there are no other dopants introduced during the experiment, the change in conductance should result from the oxygen absorption on the CdS NB surface. Once the oxygen gas molecules were introduced, they are chemisorbed onto the CdS surface at vacancy sites and recombine with the free electron, presumably forming anions and resulting in a surface negative charge depletion layer, which significantly reduces the free carrier concentration of CdS NB, therefore reducing the conductivity of CdS. In contrast, N_2 is not reactive to the surface defects, so the photocurrent is not affected by its introduction. From the thermodynamics of gas adsorption, the amount of molecules absorbed on surface and the possibility of absorption of a molecule decrease as the gas pressure decreases. Therefore, in lower oxygen partial pressures, the amount of oxygen absorbed is less, so the conductivity of CdS is higher than that at a higher oxygen partial pressure.

It should be emphasized that the current under ambient conditions is much lower than that under dry oxygen gas and the decay time constant is smaller. A similar phenomenon is observed in a wet O_2 ambient, but in a wet N_2 ambient the photocurrent is little changed. The results indicate that the condensed water on the CdS surface has a catalytic effect. It is widely accepted that when the device is exposed to the ambient, a very thin water layer will form on the sample surface. The condensed water on the surface can accelerate the oxygen adsorption process. The electron exchange from CdS NB to oxygen molecules can be described by the following reactions:

On CdS NB surface: $[V_{Cd}] + e^- \rightarrow [V_{Cd}]^-$.

Inside the condensed water: $H_2O \rightarrow H^+ + OH^-$,

$[V_{Cd}]^- + H^+ \rightarrow H^+[V_{Cd}]^-$.

On the top of the water layer: $OH^- + O_2 \rightarrow [O_2]^-_{ads}OH$.

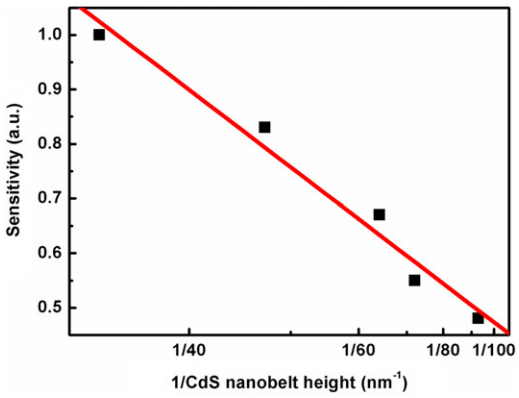

Figure 4. Oxygen sensitivity as a function of the CdS NB height (H) (solid square) and its linear fitting line (solid line).

The H_2O layer effectively occupies the surface negative acceptor-like defects (presumably cadmium vacancies V_{Cd}) on the CdS surface, because H^+ is bound with a cadmium vacancy via a single bond which needs less energy than the double bond for O_2. The thin water layer provides an effective pathway for the exchange of electrons from CdS to the oxygen molecules through a process in which the H^+ ions act as surface acceptors bound with a cadmium vacancy, thus shortening the photo response time effectively.

3.4. Oxygen sensitivity versus CdS NB geometry

We find that the oxygen sensitivity is dependent on the geometry of the CdS NBs in the dark. The $1/H$ linear relationship in figure 4 manifests that the thinner CdS NB shows a much higher sensitivity to the same oxygen molecule concentrations.

The results shown in figure 4 can be explained by the following model. Assuming a uniform charge carrier distribution inside the CdS NB, the conductance (G) can be described by:

$$G = \frac{W \times H}{L} n_0 q \mu_{\mathrm{CdS}} \tag{1}$$

where H, W and L are the height, width and length of the CdS NB respectively, n_o is the bulk electron concentration, q is the elementary charge and μ_{CdS} is the intrinsic electron mobility. For a belt-like geometry, the change in carrier concentration after introducing the gas can be described by equation (2):

$$\begin{aligned} n &= n_0 - \alpha N_{\mathrm{surface}} \frac{A \times L}{S \times L} = n_0 - \alpha N_{\mathrm{surface}} \frac{2(W+H)}{W \times H} \\ &\approx n_0 - \alpha N_{\mathrm{surface}} \frac{2}{H} \qquad (\text{for } w \gg H) \end{aligned} \tag{2}$$

where A and S are the perimeter and cross-sectional area, respectively, of the CdS NB; N_{surface} is the unit area concentration of the available surface defects/states on the CdS NB surface; and α is an absorption coefficient dependent on the oxygen partial pressure and temperature. The product of α and N_{surface} reflects the number of adsorbed oxygen molecules on the surface of CdS NB. Then, the normalized conductance change with a given change of oxygen partial pressure ($P - P_0$) at room temperature is given by

$$\frac{\Delta G}{G_0} = \frac{n_0 - n}{n_0} = \frac{\alpha(P) N_{\mathrm{surface}}}{N_0} \frac{2}{H}. \tag{3}$$

The behavior of the conductance change with the NB height observed in figure 4 just resembles the $1/H$ relationship as described in equation (3). Furthermore, the conductance change is proportional to the number of adsorbed oxygen molecules on the surface ($\alpha(P)N_{\mathrm{surface}}$) which is determined by the oxygen partial pressure.

3.5. FET performance versus oxygen ambient

The oxygen ambient effect on the conductivity of the NB is also investigated by measuring the CdS NB FET I_{DS}–V_{G} curves in the dark with controlled oxygen partial pressure. The transfer curve for a single CdS NB FET is shown in figure 5(a). The conductance of CdS NB increases with the gate voltage and the on/off ratio can exceed 10^2, which suggests that the device is a typical n-type channel depletion-mode FET. The threshold voltage (V_{T}) shifts to the positive voltage from the oxygen-deficient condition ($V_{\mathrm{T}} = -15.8$ V in the vacuum state) to the oxygen-sufficient condition ($V_{\mathrm{T}} = -1.9$ V in 100% dry oxygen conditions), which illustrates a 'p-type' doping effect: the electron carrier concentration of the CdS NB decreases once oxygen molecules are introduced.

The oxygen sensitivity $I_{\mathrm{vac}}/I_{\mathrm{oxygen}}$ (10 Pa) at different gate voltages is plotted in figure 5(b). The maximum sensitivity is obtained when V_{G} is close to the threshold voltage, since the negative gate potential nearly depletes the electron carriers in the CdS NB and reduces the potential of the NB. The available defect states on the surface decrease, since the oxygen molecules can only recombine with the defect states whose energies are less than the Fermi level. The contribution of the adsorbed oxygen molecules to the conductance is stronger when the gate voltage reaches V_{T} (the flat band voltage).

The electron density can be estimated by assuming a homogeneous electron (Q) distribution on the NB as $Q = C_{\mathrm{G}} V_{\mathrm{T}}$ [21], where C_{G} is the NB capacitance, V_{T} is the threshold gate voltage which allows the CdS NB to become fully depleted. Assuming a parallel plate model [2], given by $C_{\mathrm{G}} = \varepsilon\varepsilon_0 LW/h$, where ε is the relative dielectric constant, ε_0 is the vacuum permittivity, W is the NB width, L is the channel length ($L = 4$ μm) and h is the thickness of the dielectric layer (SiO_2), then the 1D electron density n along the CdS NB can be calculated to be 1.13×10^8 cm^{-1} in the vacuum and 1.36×10^7 cm^{-1} in an O_2 partial pressure of 10^5 Pa. The electron density (N_{d}) can be obtained by dividing the 1D electron density n by the cross-sectional area of the NB, then the values 2.84×10^{17} cm^{-3} and 3.41×10^{16} cm^{-3} can be obtained for the vacuum and O_2 partial pressure of 10^5 Pa, respectively.

The mobility of the CdS NBs can be estimated from the transconductance, $g = \frac{\mathrm{d}I_{\mathrm{DS}}}{\mathrm{d}V_{\mathrm{G}}} = \mu \frac{C_{\mathrm{G}}}{L^2} V_{\mathrm{DS}}$, the calculated mobilities are 13.69 cm^2 V^{-1} s^{-1} for the vacuum and 3.24 cm^2 V^{-1} s^{-1} for the 100% dry oxygen condition as shown in figure 5(d). The increase in electron density in the vacuum environment (figure 5(d)) originates from the release of the

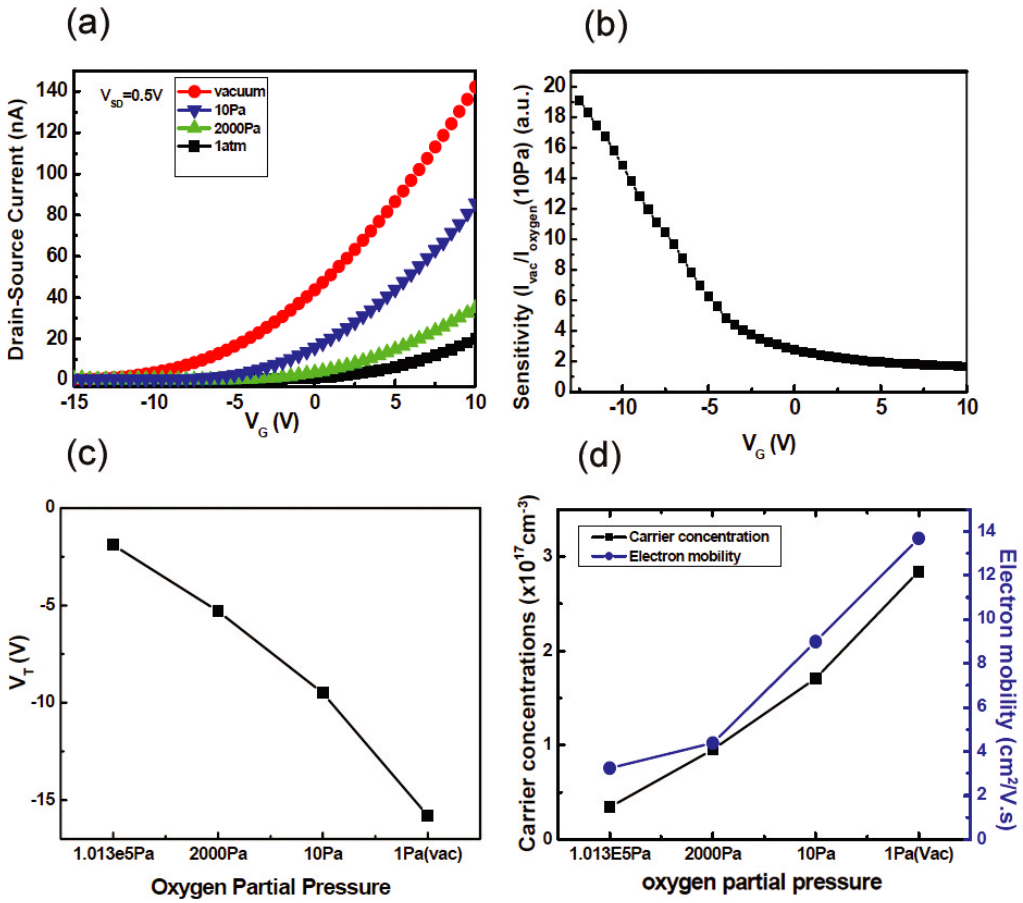

Figure 5. (a) I_{DS}–V_{GS} curves for different oxygen conditions, $V_{DS} = 0.5$ V; (b) oxygen sensitivity I_{vac}/I (10 Pa oxygen) at different gate voltages; (c) the obtained threshold voltage; (d) carrier mobility and concentration for different oxygen conditions.

surface shallow acceptors since no dopant is introduced during the pumping process. The oxygen molecules can recombine with the free electrons inside the NB, then adsorb on the available defect sites at the surface of the n-type CdS, alter the surface band and change the carrier concentration inside the CdS NB. The increase of mobility in the vacuum (figure 5(d)) can be attributed to the decrease in the number of adsorbed oxygen anions, which can act as scattering centers hindering the current flow inside the CdS NB.

The transistor performance is greatly affected by surface adsorbed oxygen molecules. (1) the electron carrier concentration increases with deficient oxygen molecules (shown in figure 5(d)) since the trapped electrons are released when the oxygen molecules are desorbed in the vacuum. (2) Carrier mobility also increases with deficient oxygen. The mobility in the vacuum is higher than that in the oxygen-rich condition partly because the adsorbed oxygen anion can act as scattering centers to hinder the current flow in CdS NB. (3) The threshold voltage (V_T) decreases in oxygen-deficient conditions, since the electron concentration is proportional to the carrier concentrations. When the sample is exposed to oxygen gas, the free electrons are recombined with the oxygen molecules to decrease the free carrier concentration. The adsorbed oxygen acts as a surface shallow acceptor, thus the threshold voltage can shift to the positive voltage side, consistent with the experimental observation.

The FET results illustrate that the oxygen adsorbent can shift V_T and decrease the free carrier concentration and mobility effectively. Since there is no other dopant, the only explanation is that the surface states of CdS change. In the oxygen-deficient environment, the adsorbed oxygen molecules undergo a desorption process and the electrons are released to become free carriers. In the oxygen-rich environment, the oxygen molecules adsorb on the CdS surface again and the carrier concentration decreases. This shows that control of the surface states is a key factor in fabricating high performance NB FETs.

3.6. Surface band bending estimated by SSPM

SSPM is used to measure the contact potential difference (CPD) between sample surface and metal coating tip. The principle and detailed experimental setup can be found elsewhere [22]. To be brief, the surface band bending Φ can be calculated using the formula

$$\phi = \phi_M - qV_{CPD} - \phi_s - \chi + \Delta E_F \quad (4)$$

where ϕ_M is the work function of the tip coating, χ is the electron affinity of the semiconductor, q is the elementary charge, ΔE_F is the energy of the Fermi level with respect to the conduction band minimum, Φs is the vacuum level shift caused

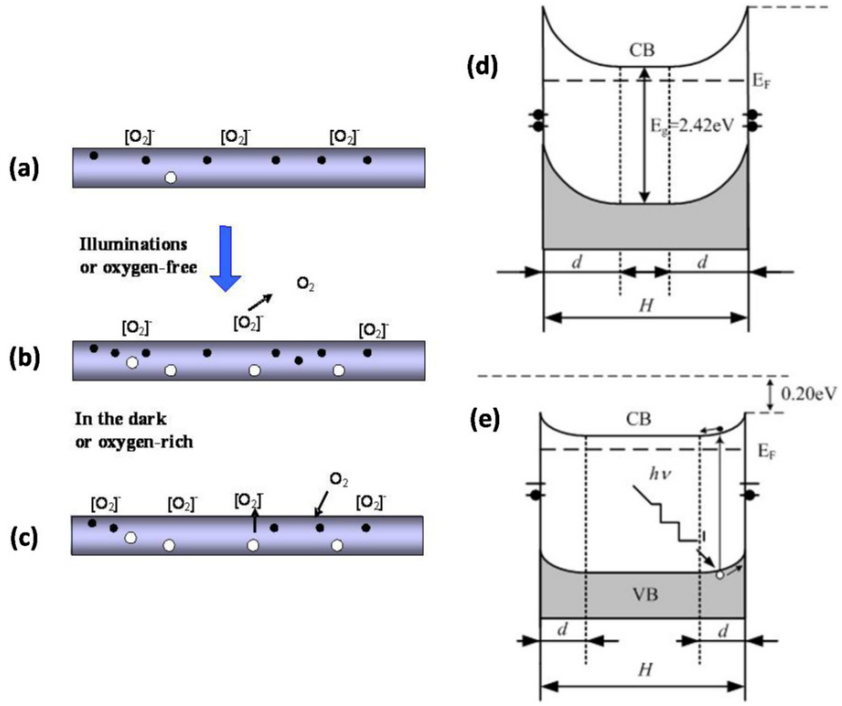

Figure 6. Schematics show the CdS NB (a) without illumination and in an oxygen-rich environment, (b) after illumination or in an oxygen-free environment and (c) in the dark or in an oxygen-rich environment. Parts (d) and (e) are corresponding band diagrams.

by the surface dipole. V_{CPD} is the contact potential difference measured from the SSPM.

SSPM performed on the CdS NBs gives an average CPD of about 0.44 eV $\pm$ 0.01 eV in the dark. The work function of the Pt/Ir-coated Si cantilever tip is 5.5 eV $\pm$ 0.1 eV (calibrated using thick gold films). Considering the electron affinity of CdS single crystal is 4.4 eV and the E_F value is just 0.2 eV below the conduction band minimum [23], we can obtain that the surface band bends upward for about 0.46 eV by using equation (4) and neglecting the dipole effect. The upward band bending demonstrates the negative charge existing on the surface of the CdS NB.

3.7. Discussion

3.7.1. Contact effect. As for the surface band bending status, the contact status may influence the measured electrical properties of the CdS NB device. The contact barrier can be Ohmic or Schottky in our experiment. It is possible that the contact resistance has taken away a portion of V_{DS} which leads to underestimation of the mobility under fixed oxygen partial pressure. The contact between Au (with a work function of 5.0) electrode and CdS (work function is 5.5 from SSPM) may be altered when exposed to the oxygen environment, e.g. dipole formation by charge transfer from the metal to the oxygen molecule [24–26], leading to a slight increase in the metal electrode work function. The barrier height between the metal and semiconductor will be reduced and the conductance should increase. So the contact effect may be reduced in higher oxygen partial pressures.

3.7.2. Surface defects where oxygen is absorbed. On the surface of CdS, defects or dangle-bonds probably form non-irradiative centers or surface related defect states. The deep electron traps (acceptor-like defects), that are often attributed to the sulfur interstitials (S_i) [27] or to cadmium vacancies(V_{Cd}) [28], are responsible to the long wavelength optical absorption and photo response. The electron trap positions were located (1) at 1.4 eV below the CdS conduction band by photo-capacitance study of a CdS Schottky diode [28], associated with a cadmium vacancy (V_{Cd}); or (2) at 1.5 eV above the valence band by photo-electrochemistry on CdS [27], probably associated with a sulfur interstitial (S_i). It is hard to elucidate which defect is responsible for the oxygen adsorption process. In fact, the electron-stimulated-desorption experiment on CdS demonstrates that both defects can adsorb oxygen adsorbates [29], and the sticking coefficient on the S-terminated face is comparable to that of Cd-terminated faces [30]. However, in the HRTEM image, a very thin amorphous layer covers the CdS NB, which is very likely an oxide layer. This illustrates that the cadmium vacancies V_{Cd} in the CdS NB may be the main surface defect sites to adsorb the oxygen molecules leading to chemisorption of oxygen species ($[O_2]^-_{ads}$).

3.7.3. Interplay of oxygen absorption/desorption with transport properties. In the oxygen-rich environment without illumination, some oxygen molecules are adsorbed on the surface of CdS (figure 6(a)), resulting in electrons filling surface states below the Fermi level, which leads to the surface band bending upwards as shown in figure 6(d). Once illuminating the CdS, the photo-generated excess holes will recombine with the adsorbed oxygen anions, $[O_2]^-_{ads} \rightarrow O_2^{\uparrow} + e^-$, and release oxygen molecules, as shown in figure 6(b). The surface band diagram is schematically shown in figure 6(e).

It can be seen that illumination will flatten the surface band bending. After turn off the illuminations, the oxygen will be adsorbed again on the surface of CdS, as shown in figure 6(c). The chemisorbed molecules can influence the conductivity in the following ways. (1) Decrease the carrier concentrations: the photo-generated holes can recombine with the surface negative oxygen adsorbates and release oxygen molecules. Thus, under vacuum more negative adsorbed oxygen will be released, and a higher carrier concentration and surface band bending will be recovered. In contrast, under an oxygen environment, oxygen will be absorbed on the CdS NB surface and deplete the surface and then decrease the carrier concentration. (2) Decrease the mobility: the adsorbed oxygen atoms will scatter the electrons and lead to the decrease of mobility.

3.7.4. Geometry shape effect on the charge transport. As we previously showed in figure 4, the oxygen sensitivity of the CdS NB has a reverse dependence on the geometry of the NB, i.e. the height of the NB plays a crucial role. The lower the height, the larger the sensitivity is. The size effects on the carrier transport properties of FETs for various nanostructures have been reported [31, 32]. It is widely observed that the smallest size or, more specifically, the smallest dimension (SD) of the cross-section, typically below 100 nm, causes their electrical properties to be very dependent on the local environment where charge changes on the surface induce a field effect that significantly alters the carrier concentration and, thus, the conductance. The reason is that most of the 1D nanostructures exhibit a depleted space charge layer with an extension of the order of the SD, i.e. height of the NB or nanoribbon and the diameter of a NW or nanorod. Depending on SD and doping, there exists a critical value for the SD—smaller than this, a completely depleted 1D nanostructure is formed and greater than this, a 1D nanostructure with thin conducting channels exists.

4. Conclusion

The effects of the oxygen environment on the carrier transport behavior for CdS NB devices are studied experimentally. It is found that the chemisorbed oxygen molecules can influence the conductivity in the following ways. (1) Decrease the carrier concentration. (2) Decrease the mobility. Both lead to a decreased conductivity. Furthermore, the conductance change of the CdS device in an oxygen environment strongly depends on the height of the NB. The lower the height is, the higher the sensitivity attained. We show that controlling the condition of the surface states is critical for the design and fabrication of future optoelectronic and electronic devices in which NWs/NBs are used.

Acknowledgments

The work is in part supported by Research Grants Council of Hong Kong, particularly, via grant nos N_CUHK447/07 and CUHK2/CRF/08. J B Xu would like to thank the National Science Foundation of China for their support, particularly via grant nos 60990314 and 60928009.

References

[1] Ma R M, Dai L, Huo H B, Xu W J and Oin G G 2007 *Nano Lett.* **7** 3300
[2] Duan X F, Niu C M, Sahi V, Chen J, Parce J W, Empedocles S and Goldman J L 2003 *Nature* **425** 274
[3] Wu P C, Ye Y, Sun T, Peng R M, Wen X N, Xu W J, Liu C and Dai L 2009 *Acs Nano* **3** 3138
[4] Duan X F, Huang Y, Agarwal R and Lieber C M 2003 *Nature* **421** 241
[5] Gu Y, Kwak E S, Lensch J L, Allen J E, Odom T W and Lauhon L J 2005 *Appl. Phys. Lett.* **87** 043111
[6] Hayden O, Agarwal R and Lieber C M 2006 *Nat. Mater.* **5** 352
[7] Chen J, Xue K, An J, Tsang S W, Ke N, Xu J B, Li Q and Wang C R 2005 *Ultramicroscopy* **105** 275
[8] Long Y, Chen Z J, Wang W L, Bai F L, Jin A Z and Gu C Z 2005 *Appl. Phys. Lett.* **86** 153102
[9] Wei T Y, Huang C T, Hansen B J, Lin Y F, Chen L J, Lu S Y and Wang Z L 2010 *Appl. Phys. Lett.* **96** 013508
[10] Jie J S, Zhang W J, Jiang Y and Lee S T 2006 *Appl. Phys. Lett.* **89** 223117
[11] Jie J S, Zhang W J, Jiang Y, Meng X M, Li Y Q and Lee S T 2006 *Nano Lett.* **6** 1887
[12] Mondal S P and Ray S K 2009 *Appl. Phys. Lett.* **94** 223119
[13] Ip K M, Wang C R, Li Q and Hark S K 2004 *Appl. Phys. Lett.* **84** 795
[14] Wang C R, Ip K M, Hark S K and Li Q 2005 *J. Appl. Phys.* **97** 054303
[15] Ahn Y, Dunning J and Park J 2005 *Nano Lett.* **5** 1367
[16] Lien D H, Hsu W K, Zan H W, Tai N H and Tsai C H 2006 *Adv. Mater.* **18** 98
[17] Balasubramanian K, Fan Y W, Burghard M, Kern K, Friedrich M, Wannek U and Mews A 2004 *Appl. Phys. Lett.* **84** 2400
[18] An J *et al* 2011 in preparation
[19] Butty J, Peyghambarian N, Kao Y H and Mackenzie J D 1996 *Appl. Phys. Lett.* **69** 3224
[20] Ong H C, Li A S K and Du G T 2001 *Appl. Phys. Lett.* **78** 2667
[21] Sze S M 1981 *Physics of Semiconductor Devices* 2nd edn (New York: Wiley)
[22] Jacobs H O, Knapp H F and Stemmer A 1999 *Rev. Sci. Instrum.* **70** 1756–60
[23] Brillson L J 1978 *Phys. Rev.* B **18** 2431
[24] Heinze S, Tersoff J, Martel R, Derycke V, Appenzeller J and Avouris P 2002 *Phys. Rev. Lett.* **89** 106801
[25] Cui X D, Freitag M, Martel R, Brus L and Avouris P 2003 *Nano Lett.* **3** 783
[26] Ishii H, Sugiyama K, Ito E and Seki K 1999 *Adv. Mater.* **11** 605
[27] Meissner D, Lauermann I, Memming R and Kastening B 1988 *J. Phys. Chem.* **92** 3484
[28] Hussein M, Lleti G, Sagnes G, Bastide G and Rouzeyre M 1981 *J. Appl. Phys.* **52** 261
[29] Ekwelundu E C and Ignatiev A 1988 *Phys. Rev.* B **38** 3671
[30] Campbell B D and He F 1968 *Surf. Sci.* **10** 197
[31] Calarco R, Marso M, Richter T, Aykanat A I, Meijers R, Hart A V, Stoica T and Luth H 2005 *Nano Lett.* **5** 981
[32] Elfstrom N, Juhasz R, Sychugov I, Engfeldt T, Karlstrom A E and Linnros J 2007 *Nano Lett.* **7** 2608